the triangular lattice depicted in Fig. 2, σ was found to be -0.1, providing evidence for the predominant antiferromagnetic nearest-neighbour coupling of the individual half-integer flux quanta in this system. For the next-nearest-neighbour interaction, at a distance of $\sim$21 μm, σ was close to 0. It is probable that the pattern of half flux quanta shown in Fig. 2 includes some frozen-in disorder, as with the used cool-down speed of about 10 mK s^{-1}, the large-scale array will not have sufficient time to relax to an overall energetic ground state. This source of disorder may be reduced by lowering the cool-down speed.

The spontaneous currents generated in the elements of the triangular array of Fig. 2 were remarkably uniform, as indicated by a full-width at half-maximum of the distribution in peak amplitudes, which was about 0.28 times the average peak height. We do not believe that this observed spread is a dominant source of disorder in the π-ring array cooling experiments, because it will cause fluctuations in the magnitude, as opposed to fluctuations in the sign, of the ring–ring coupling. A detailed comparison between the ordering in two-dimensional half-fluxon lattices generated in frustrated and unfrustrated geometries—the latter including, for example, square and honeycomb lattices—is under investigation.

Once cooled down to $T = 4.2$ K, the energy required to alter the polarity of a half flux quantum is considerably larger than the thermal energy ($E_b \approx I_c \Phi_0/\pi > 10^4$ K), which is reflected in the temporal stability of the flux pattern. But by applying locally a magnetic field, it is possible to manipulate the polarity of the individual half-integer flux quanta, enabling the possibilities of storing information or of constructing desired patterns of fractional flux. This is demonstrated in Fig. 3, showing six half-fluxons in a hexagonal arrangement, with opposite polarity to the surrounding half flux quanta in this triangular lattice, spaced at 25 μm. The polarity of the half flux quanta in this sample with facet length $a = 10$ μm was set by scanning a SQUID susceptometer[31] over the junctions at a rate of 0.05 mm s^{-1} while applying a 2-mA current through the excitation coil (this coil is 21 μm in diameter, and concentric and co-planar with the 8 μm square SQUID pick-up loop). This corresponds to a field of approximately 50 μT at the junction. Reversing the current direction reversed the resultant polarity of the half-vortex. The critical field required to flip the polarity of the half-vortex is in rough agreement with numerical calculations[32]. We expect that, apart from the spontaneous flux formation, the writing of half flux quanta patterns will provide a diverse basis for both fundamental studies and potential applications. □

Received 14 October 2002; accepted 14 January 2003; doi:10.1038/nature01442.

1. Bardeen, J., Cooper, L. N. & Schrieffer, J. R. Theory of superconductivity. *Phys. Rev.* **108,** 1175–1204 (1957).
2. Deaver, B. S. Jr & Fairbank, W. M. Experimental evidence for quantized flux in superconducting cylinders. *Phys. Rev. Lett.* **7,** 43–46 (1961).
3. Doll, R. & Näbauer, M. Experimental proof of magnetic flux quantization in a superconducting ring. *Phys. Rev. Lett.* **7,** 51–52 (1961).
4. Geshkenbein, V. B. & Larkin, A. I. The Josephson effect in superconductors with heavy fermions. *JETP Lett.* **43,** 395–399 (1986).
5. Geshkenbein, V. B., Larkin, A. I. & Barone, A. Vortices with half magnetic flux quanta in "heavy-fermion" superconductors. *Phys. Rev. B* **36,** 235–238 (1987).
6. Sigrist, M. & Rice, T. M. Paramagnetic effect in high-T_c superconductors—a hint for *d*-wave superconductivity. *J. Phys. Soc. Jpn* **61,** 4283–4286 (1992).
7. Tsuei, C. C. & Kirtley, J. R. Pairing symmetry in cuprate superconductors. *Rev. Mod. Phys.* **72,** 969–1016 (2000).
8. Bulaevskii, L. N., Kuzii, V. V. & Sobyanin, A. A. Superconducting system with weak coupling to the current in the ground state. *JETP Lett.* **25,** 290–294 (1977).
9. Van Harlingen, D. J. Phase-sensitive tests of the symmetry of the pairing state in the high-temperature superconductors—Evidence for d_{x2-y2} symmetry. *Rev. Mod. Phys.* **67,** 515–535 (1995).
10. Schulz, R. R. *et al.* Design and realization of an all *d*-wave dc π-superconducting quantum interference device. *Appl. Phys. Lett.* **76,** 912–914 (2000).
11. Smilde, H. J. H. *et al. d*-Wave-induced Josephson current counterflow in $YBa_2Cu_3O_7$/Nb zigzag junctions. *Phys. Rev. Lett.* **88,** 057004 (2002).
12. Smilde, H. J. H., Hilgenkamp, H., Rijnders, G., Rogalla, H. & Blank, D. H. A. Enhanced transparency ramp-type Josephson contacts through interlayer deposition. *Appl. Phys. Lett.* **80,** 4579–4581 (2002).
13. Aeppli, G. & Chandra, P. Seeking a simple complex system. *Science* **275,** 177–178 (1997).
14. Moessner, R. & Sondhi, S. L. Ising models of quantum frustration. *Phys. Rev. B* **63,** 224401 (2001).
15. Chandra, P. & Doucot, B. Possible spin-liquid state at large S for the frustrated square Heisenberg lattice. *Phys. Rev. B* **38,** 9335–9338 (1988).
16. Davidovic, D. *et al.* Magnetic correlations, geometrical frustration, and tunable disorder in arrays of superconducting rings. *Phys. Rev. B* **55,** 6518–6540 (1997).
17. Pannetier, B., Chaussy, J., Rammal, R. & Villegier, J. C. Experimental fine tuning of frustration: Two-dimensional superconducting networks in a magnetic field. *Phys. Rev. Lett.* **53,** 1845–1848 (1984).
18. Lerch, Ph., Leemann, Ch., Theron, R. & Martinoli, P. Dynamics of the phase transition in proximity-effect arrays of Josephson junctions at full frustration. *Phys. Rev. B* **41,** 11579–11582 (1990).
19. Mooij, J. E. *et al.* Josephson persistent-current qubit. *Science* **285,** 1036–1039 (1999).
20. Van der Wal, C. *et al.* Quantum superposition of macroscopic persistent-current states. *Science* **290,** 773–777 (2000).
21. Friedman, J. R., Patel, V., Chen, W., Tolpygo, S. K. & Lukens, J. E. Quantum superposition of distinct macroscopic states. *Nature* **406,** 43–46 (2000).
22. Ioffe, L. B., Geshkenbein, V. B., Feigel'man, M. V., Fauchère, A. L. & Blatter, G. Environmentally decoupled sds-wave Josephson junctions for quantum computing. *Nature* **398,** 679–681 (1999).
23. Blais, A. & Zagoskin, A. Operation of universal gates in a solid-state quantum computer based on clean Josephson junctions between *d*-wave superconductors. *Phys. Rev. A* **61,** 042308 (2000).
24. Preskill, J. Reliable quantum computers. *Proc. R. Soc. Lond. A* **454,** 385–410 (1998).
25. Bennett, C. H. & DiVincenzo, D. P. Quantum information and computation. *Nature* **404,** 247–255 (2000).
26. Rogers, F. P. *A Device for Experimental Observation of Flux Vortices Trapped in Superconducting Thin Films*. Thesis, MIT, Boston (1983).
27. Vu, L. N. & Van Harlingen, D. J. Design and implementation of a scanning SQUID microscope. *IEEE Trans. Appl. Supercond.* **3,** 1918–1921 (1993).
28. Black, R. C. Magnetic microscopy using a liquid nitrogen cooled $YBa_2Cu_3O_7$ superconducting quantum interference device. *Appl. Phys. Lett.* **62,** 2128–2130 (1993).
29. Kirtley, J. R. *et al.* High-resolution scanning SQUID microscope. *Appl. Phys. Lett.* **66,** 1138–1140 (1995).
30. Cowley, J. M. An approximate theory of order in alloys. *Phys. Rev.* **77,** 669–675 (1950).
31. Gardner, B. W. *et al.* Scanning superconducting quantum interference device susceptometry. *Rev. Sci. Instrum.* **72,** 2361–2364 (2001).
32. Kirtley, J. R., Moler, K. A. & Scalapino, D. J. Spontaneous flux and magnetic-interference patterns in 0-π Josephson junctions. *Phys. Rev. B* **56,** 886–891 (1997).

Acknowledgements We thank R. H. Koch, J. Mannhart, D. M. Newns and D. J. Scalapino for discussions. This work was supported by the Dutch Foundation for Research on Matter (FOM), the Netherlands Organization for Scientific Research (NWO), the Royal Dutch Academy of Arts and Sciences (KNAW) and the European Science Foundation (ESF) PiShift programme.

Competing interests statement The authors declare that they have no competing financial interests.

Correspondence and requests for materials should be addressed to H.H. (e-mail: H.Hilgenkamp@utwente.nl).

Superconductivity in two-dimensional CoO_2 layers

Kazunori Takada*‡, Hiroya Sakurai†, Eiji Takayama-Muromachi†, Fujio Izumi*, Ruben A. Dilanian* & Takayoshi Sasaki*‡

** Advanced Materials Laboratory, National Institute for Materials Science, Tsukuba, Ibaraki 305-0044, Japan*
† Superconducting Materials Center, National Institute for Materials Science, Tsukuba, Ibaraki 305-0044, Japan
‡ CREST, Japan Science and Technology Corporation

Since the discovery of high-transition-temperature (high-T_c) superconductivity in layered copper oxides[1], many researchers have searched for similar behaviour in other layered metal oxides involving 3*d*-transition metals, such as cobalt and nickel. Such attempts have so far failed, with the result that the copper oxide layer is thought to be essential for superconductivity. Here we report that $Na_xCoO_2{\cdot}yH_2O$ ($x \approx 0.35$, $y \approx 1.3$) is a superconductor with a T_c of about 5 K. This compound consists of two-dimensional CoO_2 layers separated by a thick insulating layer of Na^+ ions and H_2O molecules. There is a marked resemblance in superconducting properties between the present material and high-T_c copper oxides, suggesting that the two systems have similar underlying physics.

The $Na_xCoO_2{\cdot}yH_2O$ sample was obtained through a chemical

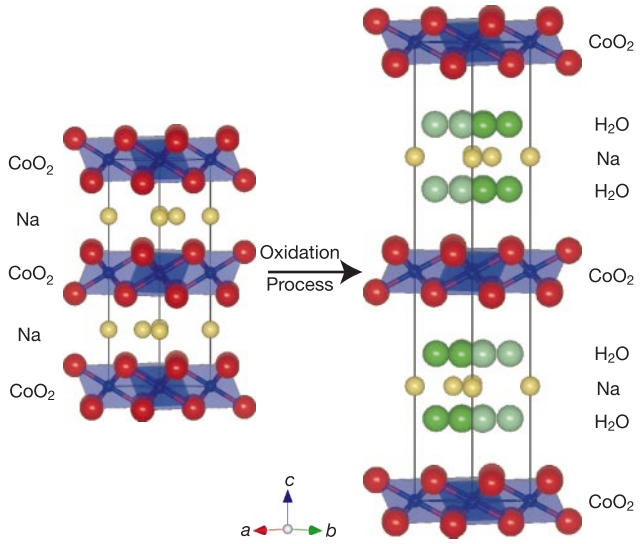

Figure 1 Structural views of $Na_{0.7}CoO_2$ (left) and $Na_xCoO_2 \cdot yH_2O$ (right), where Na and H_2O sites are partially occupied. $Na_{0.7}CoO_2$ was prepared from Na_2CO_3 (99.99%) and Co_3O_4 (99.9%) by solid-state reaction at 800 °C for 8 h under oxygen gas flow. A fivefold excess of Br_2 regarding the Na content was dissolved in acetonitrile (CH_3CN). A well pulverized powder of $Na_{0.7}CoO_2$ was immersed in the Br_2/CH_3CN solution for 5 days to deintercalate Na^+ ions; then the product was filtered, washed with CH_3CN and distilled water, and finally dried in an ambient atmosphere. No impurities were detected by energy dispersive X-ray analysis (EDX).

oxidation process (hereafter referred to as the 'oxidation process') from a parent compound of $Na_{0.7}CoO_2$ (ref. 2). Before the oxidation process, $Na_{0.7}CoO_2$ has a hexagonal layered structure (space group $P6_3/mmc$) consisting of the two-dimensional (2D) layers of CoO_2 and charge-balancing Na^+ ions (see the left side of Fig. 1)[3]. Figure 2 shows an X-ray diffraction (XRD) pattern of the product obtained through the oxidation process. All the reflections of the product

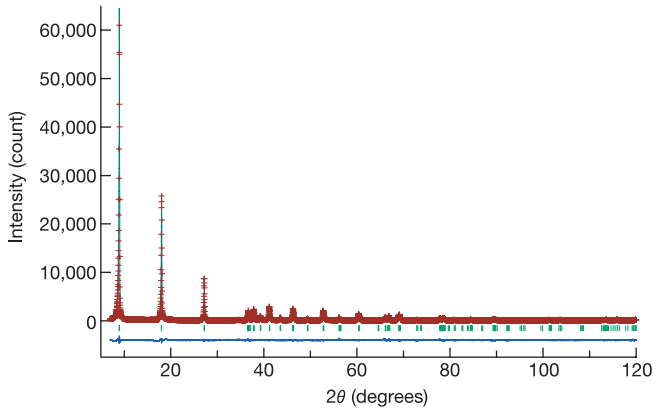

Figure 2 Rietveld refinement patterns for $Na_xCoO_2 \cdot yH_2O$. The observed diffraction intensities are represented by red plus signs, and the calculated pattern by the green solid line. The blue curve at the bottom represents the weighted difference, $(Y_{io} - Y_{ic})/\sigma$, where Y_{io}, Y_{ic} and σ are the observed and calculated intensities and the statistical uncertainty of the ith point, respectively. The differences were multiplied by 20 to make the plots easier to read. Short light green vertical bars below the observed and calculated patterns indicate the positions of allowed Bragg reflections. Powder XRD was performed by an X-ray diffractometer (RINT-2100S, Rigaku) using CuK_α radiation. The oxidation process slightly decreased a from 2.8292(3) Å for the parent compound to 2.8230(2) Å, where the parentheses indicate standard deviations, probably because Co^{3+} ions were partially oxidized to smaller Co^{4+} ions. On the other hand, c increased dramatically from 10.9628(8) Å to 19.6207(14) Å.

Table 1 **Structure parameters of $Na_xCoO_2 \cdot yH_2O$**

Atom	Site	x	y	z	g	U (Å^2)
Co	2*a*	0	0	0	1	0.0063(6)
O	4*f*	1/3	2/3	0.0451(3)	1	0.0162(12)
Na1	2*d*	2/3	1/3	1/4	0.159(4)	= *U*(O)
Na2	2*b*	0	0	1/4	0.192*	= *U*(O)
WO1†	12*k*	0.174(13)	= 2*x*(WO1)	0.1793(2)	0.070(12)	= *U*(O)
WO2†	12*k*	0.370(12)	= *x*(WO2)/2	= *z*(WO1)	0.176(12)	= *U*(O)

Space group: $P6_3/mmc$; $a = 2.8230(2)$ Å and $c = 19.6207(14)$ Å; $R_{wp} = 11.58\%$ ($\chi^2 = 4.70$), $R_{F^2} = 2.84\%$ and $R_F = 3.53\%$. g, occupancy; U, isotropic displacement parameter; x, y and z, fractional coordinates.
*The total Na content x was fixed at 0.351, which was determined by ICP-AES.
†WO denotes an H_2O molecule, whose atomic scattering factors were set equal to the sums of those of one O and two H atoms.

were indexable on the basis of space group $P6_3/mmc$. A marked increase in c was observed, which supports the idea that the intercalation of certain 'guest' molecules occurred in the oxidation process in addition to the deintercalation of Na^+ ions. H_2O is the most probable candidate for the guest. The composition calculated on this assumption from Na and Co contents determined by inductively coupled plasma atomic-emission spectrometry (ICP-AES) was $Na_{0.35}CoO_2 \cdot 1.3H_2O$. In addition, the analysis of species evolved from heated samples by infrared spectroscopy showed that the H_2O content was 1.24 per formula unit.

Next, we carried out Rietveld analysis[4] of the XRD data, adopting a structural model shown in the right side of Fig. 1. In this model, H_2O molecules were located at 12*k* sites on the basis of electron-density distribution obtained by a maximum-entropy method[4]. Table 1 lists the final structure parameters, and Fig. 2 shows Rietveld refinement patterns. The resulting H_2O content was 1.47 per formula unit, which is close to the analytical values. The final R factors were fairly low, which provides evidence for the validity of our present structural model.

The magnetic susceptibility (χ) of $Na_xCoO_2 \cdot yH_2O$ is plotted in Fig. 3 as a function of temperature. In the measurements under the external magnetic field $H = 20$ Oe, a steep decrease of susceptibility was observed at about 5 K both in the zero-field cooling and field cooling processes. The χ at 2 K in the field cooling process was -1.6×10^{-3} e.m.u. g^{-1}, which was 6.5% of the theoretical value for perfect diamagnetism. Twice-as-large diamagnetism ($\chi = -3.4 \times 10^{-3}$ e.m.u. g^{-1}, 13% of the theoretical value) was

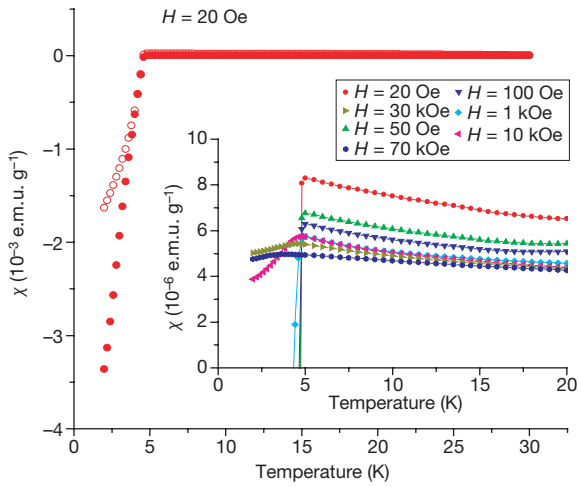

Figure 3 Magnetic susceptibility (χ) of $Na_xCoO_2 \cdot yH_2O$. Filled circles, zero-field cooling; open circles, field cooling. The susceptibility was measured in a magnetic field of 20 Oe. The inset shows χ measured under various magnetic fields by the zero-field cooling process. The magnetization was measured by a superconducting quantum interference device (SQUID) magnetometer (MPMS XL, Quantum Design).

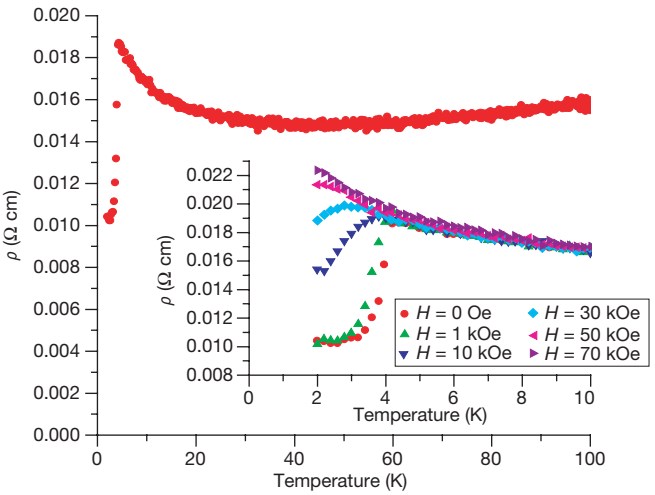

Figure 4 Resistivity (ρ) of $Na_xCoO_2 \cdot yH_2O$ under zero magnetic field. The inset figure shows the resistivity measured under various magnetic fields. The electric resistivity was measured on a compressed powder sample by a standard four-probe method using a physical property measurement system (PP700C1, Quantum Design).

observed in the zero-field cooling process. We conclude that the present phase undergoes superconducting transition at about 5 K, because only superconductivity can account for such a large diamagnetism. With increasing H to 1 kOe, the onset temperature of superconductivity (onset T_c) did not change noticeably. With further increase of H up to 70 kOe, downturn of the susceptibility was still observed near 5 K, but the superconducting transition became quite broad and susceptibility was not negative even at 2 K. The M (magnetization)–H curve at 2 K, which is not shown here, indicated that the present material is a superconductor of the second kind with a lower critical field of around 100 Oe. The normal-state susceptibility depended on temperature, and decreased with increasing external magnetic field. $Na_{0.5}CoO_2$ shows Curie–Weiss-like magnetic behaviour rather than Pauli paramagnetic behaviour[5]. This suggests that the aforementioned normal-state magnetism reflects the intrinsic nature of the CoO_2 layer, although there is a possibility that the present sample contained a trace amount of magnetic impurity.

The electric resistivity (ρ) of $Na_xCoO_2 \cdot yH_2O$ is shown in Fig. 4. For the present system, it was impossible to prepare a tightly sintered ceramic specimen for the resistivity measurement. Instead, we measured a specimen obtained by room-temperature compression, and zero resistivity was not attained down to 2 K owing to this limitation. Nevertheless, a sharp decrease of resistivity was observed at around 4 K, supporting the superconducting transition. The onset temperature of 4 K is slightly lower than the value determined by the magnetic measurement, and this difference may be due to the variation of water content in the sample. The H_2O content was dependent on the humidity in the atmosphere, and superconductivity was greatly suppressed in a low H_2O-content sample. The superconducting transition became broad with an increasing magnetic field, as shown in Fig. 4, and no decline of resistivity was observed above 50 kOe. This presumably reflects the weak link nature of the specimen. It is, however, worth noting that the onset T_c does not appear to depend significantly on the magnetic field. For instance, onset T_c at 10 kOe was very close to that under zero field.

There is a marked resemblance between the present cobalt oxide and high-T_c copper oxides. In the high-T_c copper oxides, superconductivity occurs in the CuO_2 square lattice. The Cu^{2+} ($S = 1/2$) moments are antiferromagnetically ordered in the CuO_2 plane. With a low level of carrier (hole or electron) doping, the antiferromagnetism is suppressed drastically, and the system becomes metallic, followed by the appearance of superconductivity. By analogy, the present material may be understood to be an electron-doped system for a low-spin Co^{4+} ($S = 1/2$) lattice with an electron density (x in $Na_xCoO_2 \cdot yH_2O$) of around 0.35 per Co atom. As shown in Figs 3 and 4, the increasing external magnetic field broadened the superconducting transition but did not markedly lower the onset T_c. Similar behaviour is always observed in high-T_c copper oxides.

The strong 2D character of the layered copper oxides is believed to be important in superconductivity. In the same way, the large separation of the CoO_2 layers by the introduction of H_2O molecules seems to be essential for inducing superconductivity in the present material (superconductivity is greatly suppressed by the removal of water, accompanied by a shrinkage of the c axis). The main difference between the two systems is that Co ions form a triangular lattice with magnetically frustrated geometry in contrast to the square lattice of the CuO_2 plane. Further studies are needed to elucidate the mechanism of superconductivity. □

Received 18 October 2002; accepted 28 January 2003; doi:10.1038/nature01450.

1. Bednorz, J. G. & Müller, K. A. Possible high T_c superconductivity in the Ba-La-Cu-O system. *Z. Phys. B* **64,** 189–193 (1986).
2. Fouassier, C., Matejka, G., Reau, J.-M & Hagenmuller, P. Sur de nouveaux bronzes oxygènès de formule Na_xCoO_2 ($x \leq 1$). Le system cobalt-oxygène-sodium. *J. Solid State Chem.* **6,** 532–537 (1973).
3. Balsys, R. J. & Davis, R. L. Refinement of the structure of $Na_{0.74}CoO_2$ using neutron powder diffraction. *Solid State Ionics* **93,** 279–282 (1996).
4. Izumi, F. & Ikeda, T. A Rietveld-analysis program RIETAN-98 and its applications to zeolites. *Mater. Sci. Forum* **321–324,** 198–203 (2000).
5. Tanaka, T., Nakamura, S. & Iida, S. Observation of distinct metallic conductivity in $NaCo_2O_4$. *Jpn J. Appl. Phys.* **33,** L581–L582 (1994).

Acknowledgements We thank Y. Yajima, S. Takenouchi and H. Komori of our institute for IR, ICP-AES and EDX analysis.

Competing interests statement The authors declare that they have no competing financial interests.

Correspondence and requests for materials should be addressed to K.T. (e-mail: takada.kazunori@nims.go.jp).

Dynamical coupling of wind and ocean waves through wave-induced air flow

T. S. Hristov*, S. D. Miller† & C. A. Friehe†‡

** Department of Earth and Planetary Sciences, Johns Hopkins University, Baltimore, Maryland 21218, USA*
† Department of Earth System Science, ‡ Department of Mechanical and Aerospace Engineering, University of California, Irvine, California 92697, USA

Understanding the physical mechanisms behind the generation of ocean waves by wind has been a longstanding challenge[1,2]. Previous studies[3–6] have assumed that ocean waves induce fluctuations in velocity and pressure of the overlying air that are synchronized with the waves, and numerical models have supported this assumption[7]. In a complex feedback, these fluctuations provide the energy for wave generation. The spatial and temporal structure of the wave-induced airflow therefore holds the key to the physics of wind–wave coupling, but detailed observations have proved difficult. Here we present an analysis of wind velocities and ocean surface elevations observed over the open ocean. We use a linear filter[8] to identify the wave-induced